Available online at www.sciencedirect.com
ScienceDirect
Geochimica et Cosmochimica Acta 71 (2007) 3348–3360
Geochimica et Cosmochimica Acta
www.elsevier.com/locate/gca

The composition of liquids coexisting with dense hydrous magnesium silicates at 11–13.5 GPa and the endpoints of the solidi in the $MgO–SiO_2–H_2O$ system

Elena Melekhova [a,*], Max W. Schmidt [a,*], Peter Ulmer [a], Thomas Pettke [b]

[a] *Institute of Mineralogy and Petrology, ETH Zurich, Clausiusstrasse 25, CH-8092 Zurich, Switzerland*
[b] *Institute of Geological Sciences, University of Bern, Baltzerstrasse 1+3, CH-3012 Bern, Switzerland*

Received 9 January 2007; accepted in revised form 27 March 2007; available online 20 April 2007

Abstract

High-pressure liquids in the $MgO–SiO_2–H_2O$ (MSH) system have been investigated at 11 and 13.5 GPa and between 1000 and 1350 °C. A bulk composition more magnesian than the tie-line forsterite–H_2O was employed for the study. Rocking multi-anvil experiments were combined with a diamond trap set-up. After termination of the experiments, the liquid trapped in the diamond layer was analysed by laser ablation ICP-MS using the 'freezing' technique. At 11 GPa, liquids coexist with one or two of phase A, clinohumite, chondrodite, and forsterite. A marked discontinuity in the evolution of liquid compositions near 1100 °C is observed at 11 GPa. A step of ~13 wt% H_2O and 13 wt% MgO is interpreted to result from overstepping the fluid-saturated solidus reaction mass balanced to 1.00(18) phase A + 1.07(4) fluid = 0.63(15) chondrodite + 1.44(2) melt. At 13.5 GPa liquids coexist with one or two of hydrous wadsleyite, clinohumite, superhydrous B, phase B, and forsterite. The discontinuity in liquid composition is no longer present, indicating that the second critical endpoint of the solidus has been overstepped. Thus, hydrous melts in the Mg-rich part of the MSH system (molar bulk Mg/Si > 2) are chemically distinct from aqueous fluids at pressure up to 11 GPa. Convergence of fluid and melt compositions along the solidus resulting in a supercritical liquid occurs between 11 and 13.5 GPa, at which pressure the entire MSH system becomes supercritical.

1. INTRODUCTION

In recent years there has been considerable interest in both the nature and the conditions of the formation and liberation of liquids from subducting oceanic lithosphere. Several volatile components ascend into the overlying mantle during subduction. Among these, H_2O is the most abundant component and also by far the best solvent. Thus, H_2O controls the properties of most subduction liquids. Increasing H_2O ionization with increasing pressure and temperature enhances the solute concentration in the liquid (Holzapfel and Franck, 1966; Manning, 2004). Such highly ionized liquids are efficient transfer agents. Therefore, a better understanding of liquid chemistry helps to elucidate the chemical evolution of the Earth's interior.

There is particular petrologic interest in the occurrence of supercritical liquids. Under appropriate conditions, solute concentrations in the fluids become so high that hydrous silicate melt and aqueous fluid become completely miscible. Such supercritical behaviour has been demonstrated experimentally for albite, quartz, and for granitic and basaltic systems (Kennedy et al., 1962; Paillat et al., 1992; Stalder et al., 2000; Kessel et al., 2005b), and it has been shown that fully miscible (supercritical) liquids in equilibrium with a basaltic solid residue have transport capabilities also at the low temperatures which are similar to subcritical melts at subduction zone pressure–temperature conditions (Kessel et al., 2005a).

In petrology, the $MgO–SiO_2–H_2O$ system (MSH) is employed as a first approximation of a natural peridotite. Investigations of liquids in this system have been conducted

* Corresponding authors.
E-mail addresses: elena.melekhova@erdw.ethz.ch (E. Melekhova), max.schmidt@erdw.ethz.ch (M.W. Schmidt).

0016-7037/$ - see front matter © 2007 Elsevier Ltd. All rights reserved.
doi:10.1016/j.gca.2007.03.034

up to 10.5 GPa. Nakamura and Kushiro (1974) showed that a fluid in equilibrium with forsterite and enstatite at 1.5 GPa, 1310 °C dissolves more silica than magnesia on a molar basis. Ryabchikov et al. (1982) indicated that at 3 GPa, 1100 °C the molar Mg/Si ratio becomes 1.0 and fluids coexisting with forsterite and enstatite dissolve more than 30 wt% of silicate components. Kawamoto et al. (2004), based on their experiments and previous investigations, presume that the Mg/Si ratio of aqueous fluid coexisting with enstatite and forsterite changes rapidly from silica-rich to magnesia-rich at around 3 GPa, 1000 °C due to an inferred structural change of liquid water.

High-pressure liquids in the MSH system were further investigated by Stalder et al. (2001) and Mibe et al. (2002). In the MSH system, Stalder et al. (2001) were the first to apply a diamond layer to trap liquids and to analyse the quench precipitate in the trap by laser ablation ICP-MS. Experiments were performed on a bulk composition corresponding to serpentine ($Mg_3Si_2O_5(OH)_4$) at 6–10.5 GPa and 900–1250 °C. Mibe et al. (2002) constrained the composition of liquids coexisting with forsterite and enstatite indirectly through chemographical analysis. Most of Mibe's experiments were performed at 1100 °C, 3–10 GPa. Both studies showed that with increasing pressure, liquid becomes enriched in magnesium reaching an MgO/SiO_2 ratio of approximately 1.5 at 10 GPa. Stalder et al. (2001) found an abrupt increase in both SiO_2 and MgO-contents above 1100 °C, 6 and 9 GPa and concluded that the wet solidus, causing a large step in the H_2O-content of the liquid phase, still exists at these pressures.

In spite of very similar MgO/SiO_2 ratios, Stalder et al. (2001) and Mibe et al. (2002) found quite different silicate solubilities at 1100 °C and 6–9 GPa. Mibe et al. (2002) reported silicate solubilities 50% smaller than those of Stalder et al. (2001), arguing that at 5 GPa, the critical endpoint of the solidus had already been overstepped. Thus the question, at which pressure the peridotite MSH model system becomes supercritical remains uncertain (see discussion of Mibe et al., 2004, and Stalder, 2004).

In this work, we present results on the liquid chemistry in the MSH system at 11 and 13.5 GPa, applying an improved diamond-trap experimental set-up directly determining H_2O-contents of the liquid phase. The endpoint of the solidus and supercritical liquids in this system are subsequently discussed. We review prior work and show that, taking appropriate experimental errors into account, almost all previous work and in particular the experimental results from Stalder et al. (2001) and Mibe et al. (2002) are coherent and can be easily reconciled. Furthermore, we demonstrate that the latter experimental data sets are consistent with an endpoint of the MSH solidus near 11–12 GPa.

Terminologically, we use the term 'liquid' as not discriminative between the 'fluid' and 'melt'. 'Fluid' refers to an aqueous solution with relatively low solute-content (supercritical with respect to the first endpoint of the H_2O system) and 'melt' to a hydrous silicate melt dominated by silicate components. 'Supercritical liquid' is used to describe the liquid phase beyond the second endpoint of the appropriate solidus. Vapour is employed for the gas phase of H_2O below the critical point of the H_2O system. Further on in this study we always use weight ratios to describe liquid compositions, for comparison, MgO/SiO_2 ratios are 0.67 for enstatite and 1.34 for forsterite.

2. EXPERIMENTAL PROCEDURE AND ANALYTICAL TECHNIQUE

Experiments were performed in a 600-ton Walker-type rocking multi-anvil device at 11 and 13.5 GPa, at temperatures between 1000 and 1350 °C. The multi-anvil module and press was rotated by 180° during the experiments in order to induce convection in the liquid, thus improving attainment of equilibrium and reducing chemical zonation within the capsule (Schmidt and Ulmer, 2004). Each experiment was rotated every 30 s within the first 30 min and every 15 min for the remaining duration of the experiment. This procedure is based on the results of a time series which showed that zonation is mainly formed during an initial phase when most of the starting material recrystallizes to form the equilibrium phases, after which there is a period of grain maturation generating much less chemical zonation. Experiments were terminated by turning off the heating power, yielding rapid quench (>200 °C/s) followed by 16–21 h of pressure unloading.

Tungsten carbide cubes with a truncation edge length (TEL) of 8 mm in combination with prefabricated MgO-octahedra of 14 mm edge length (14/8 assembly) were employed for all experiments. Natural pyrophyllite gaskets were used. The furnace assembly consists of a ZrO_2 sleeve, a stepped $LaCrO_3$ heater, and molybdenum disks/rings with inner MgO pieces.

Pressure was calibrated based on the coesite–stishovite (9.3 GPa, 1200 °C Yagi and Akimoto, 1976; Zhang et al., 1996) and forsterite–wadsleyite (14.5 GPa, 1400 °C Morishima et al., 1994) transitions. Temperature was measured with $Pt_{94}Rh_6$–$Pt_{70}Rh_{30}$ B-type thermocouples. Pressure was kept to ±1 ton of applied load and temperature was stable within ±3 °C. The thermocouple emf was not corrected for the effect of pressure. Sample containers were Au capsules fabricated from tubes with an outer diameter of 2.0 mm. Welded capsules were pressed into a cylindrical shape with 1.8 mm outer diameter and 2.5–2.7 mm length. At temperatures close to Au melting, $Au_{90}Pd_{10}$ alloys were employed.

The starting material consisted of an 85:15 molar mixture of synthetic brucite and SiO_2 (99.9%) placing the bulk composition to the MgO-rich side of the forsterite–H_2O tie-line. Quartz was ground under ethanol in an agate mortar for 40 min and dried in a Pt crucible at 1000 °C for 1 h. Brucite is a very good absorbent of H_2O and CO_2 from the environment. Therefore, before using it as a reagent in a starting material, it was dried at 120 °C in a vacuum furnace for several hours. In order to quantify the amount of fluid contained in the diamond trap by LA-ICP-MS, we used Cs as an internal standard, doping our starting material with 860 ppm of Cs in form of a CsOH solution that was subsequently dried off (details in Kessel et al., 2004). The uncertainty on the amount of Cs in every experiment is about 6% based on replicate analyses of several aliquots

by solution ICP-MS. Capsules were filled with ~2.5 mg starting material followed by a ~2 mg diamond layer, covered by another layer of starting material of ~2.5 mg. H_2O was entirely contained in brucite; the water-content of the system was about 22.7 wt% (26.4 wt% SiO_2, 50.9 wt% MgO).

The diamond trap was constituted by synthetic diamonds with a grain diameter of about 20 μm. Experiments were analysed following the "freezing" approach (Kessel et al., 2004). Briefly, the recovered, intact capsule is mounted in a brass holder being part of a freezing stage which is cooled by pumping liquid nitrogen through the brass holder in a dry argon atmosphere working hood. The frozen capsule in the brass holder is then cut open longitudinally with a razor blade, the external standard glass NIST SRM610 is added, the ablation chamber is added, closed, and then the ensemble is transferred to the laser ablation stage. Argon gas was continuously flushed across the ablation chamber glass to prevent ice formation, to maintain clear visibility of the capsule through the microscope, and to assure maximum laser beam transmission onto the sample surface. With this method, solid ice is ablated with the laser and thus problems related to fractionation of quench precipitate and fluid due to H_2O-loss upon opening of the capsule are avoided.

The diamond trap was located in reflected light mode. At least 10 pits of commonly 40–60 μm diameter were shot along the diamond layer using an energy-homogenized 193 ArF laser system (Geolas, Lambda Physik, Germany, Gunther et al., 1997). The aerosol was analysed in an Elan 6100 DRC ICPMS (Perkin-Elmer, USA) in normal mode. Fig. 1 shows a typical cross-section of a capsule after laser ablation analysis (experiment EM105). As evident from Fig. 1, the diamond layer has sharp borders and recognition of the layer did not pose any problems. Analytical conditions were very similar to those reported in Pettke et al. (2004). Laser energies of ca. 15–20 J/cm^2 ensured controlled ablation of the ~20 μm sized diamonds and the frozen interstitial fillings of the trap.

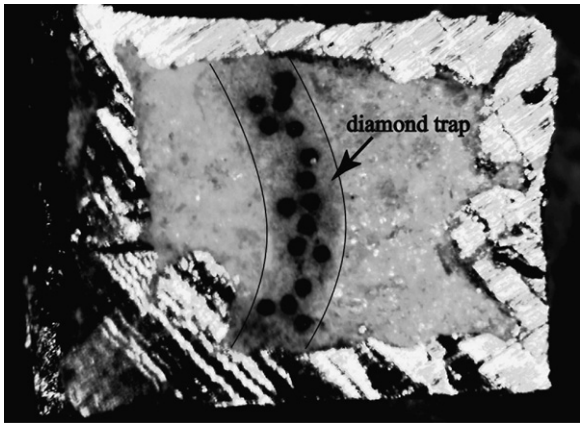

Fig. 1. Section of a capsule (experiment EM105, 13.5 GPa, 1100 °C) cut open by a razor blade while frozen in the freezing stage for the LA-ICP-MS. Black holes are laser ablation pits from ICP-MS analysis. The capsule is 1.8 mm in diameter and 2.8 mm in length.

We analysed the diamond trap for ^{25}Mg, ^{29}Si and ^{133}Cs. Data reduction followed procedures described in Longerich et al. (1996), using SRM610 glass for external standardization, and bracketing standardization for linear drift correction. Kessel et al. (2004) showed that >99.9% of the Cs added to the initial starting material exclusively partitioned into the liquid during the experiments. For our system, this was confirmed by analysing solid phases, in all of which Cs was below detection limit (⩽1 ppm). The measured Cs-concentration in the frozen trap then allows calculating the H_2O-content in the fluid. The atomic H:Cs ratio in the starting material is known (see Kessel et al., 2004, for details), and after subtracting the hydrogen contained in the hydrous solid phases, the hydrogen concentration of the fluid can be calculated. The hydrogen incorporated in the solid hydrous phases was calculated through iterative mass balance, employing stoichiometric amounts of hydrogen for phase A, B, superhydrous B, clinohumite, and chondrodite; and 2.14 wt% for wadsleyite (deduced from microprobe totals).

Uncertainties in the fluid composition were calculated by error propagation of the uncertainty in the amount of Cs (6%) and standard deviations of LA-ICP-MS measurements of each experiment. These uncertainties lead to the uncertainties on the amount of H_2O, MgO and SiO_2 in the liquids, which are all dominated by the heterogeneity measured in the 10–16 different ablation spots of each sample.

After LA-ICP-MS analysis, the capsules were mounted into epoxy resin and polished. The prepared samples were examined by electron microprobe (EMPA, JXA 8200) analysis and, if necessary, by micro-Raman (Dilor Labram II) spectroscopy to identify the solid assemblages present during run conditions. Beam conditions for EMPA were set to 10 kV and 20 nA. Forsterite was used as a standard. Data were processed with a PZAF correction procedure.

3. RESULTS

3.1. Solid residues

Experimental conditions and results are listed in Table 1. Solid phases involve rapidly changing mineral assemblages as characteristic for the investigated pressure–temperature region (see also Komabayashi and Omori, 2006) and include several humite and 'alphabet' dense hydrous magnesium silicate (DHMS) phases in addition to forsterite, namely wadsleite, clinohumite, phase A, chondrodite, phase B, and superhydrous phase B. In some experiments, additional magnesite was present in small quantities.

In all runs, the silicate phases are distributed homogeneously throughout the capsule, testifying to the effectiveness of the rocking procedure for keeping a charge homogeneous. An example of a back-scattered electron (BSE) image of the experiment at 11 GPa, 1050 °C (EM111) is shown in Fig. 2.

Where magnesite was observed in addition, these crystals were usually present as a few big grains (Fig. 2) mostly located at the contact with the diamond layer. There are three possible sources of CO_2 in our experiments. One is

Table 1
Experimental conditions and results

Experiment number	T (°C)	P (GPa)	Duration (h)	Residual phases	Fluid/melt composition, wt%		
					MgO	SiO_2	H_2O
EM113	1000	11	4	cHu + phA	16.7 ± 7.3	2.8 ± 1.1	80.4 ± 7.3
EM111	1050	11	4	phA + chond	20.9 ± 2.6	3.4 ± 0.8	75.6 ± 3.2
EM97	1100	11	5	phA + chond	32.6 ± 2.6	5.5 ± 0.6	61.8 ± 3.1
EM110	1150	11	3.1	chond	36.7 ± 4.0	4.4 ± 0.4	58.9 ± 4.0
EM109	1200	11	2	Fo	36.7 ± 1.0	5.3 ± 0.8	57.3 ± 1.9
EM103	1350	11	2	cHu + Fo	45.5 ± 2.0	12.1 ± 0.5	42.4 ± 2.7
EM107	1000	13.5	3	phA + hyW	34.6 ± 1.4	5.6 ± 0.6	59.8 ± 1.5
EM104	1050	13.5	3.3	phA + hyW	32.9 ± 2.7	7.5 ± 0.7	59.6 ± 3.3
EM105	1100	13.5	2.3	cHu + phA	37.9 ± 3.3	8.0 ± 0.8	54.1 ± 3.8
EM98	1150	13.5	4	sB + Fo	39.2 ± 2.0	9.8 ± 1.0	51.0 ± 2.0
EM106	1200	13.5	2	phB + Fo	38.2 ± 2.0	7.3 ± 0.3	54.5 ± 2.2
EM90	1250	13.5	4.20	phB + Fo	35.8 ± 5.0	11.2 ± 2.0	53.0 ± 6.0

cHu, clinohumite; chond, chondrodite; phA, phase A; Fo, forsterite; hyW, hydrous wadsleite; sB, superhydrous B; phB, phase B.

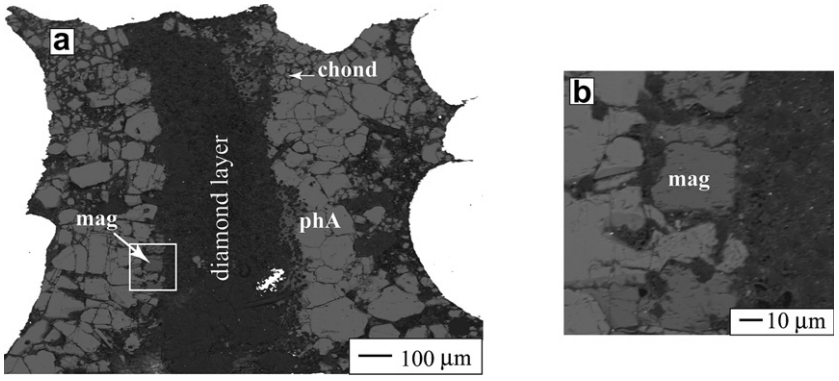

Fig. 2. Backscatter electron image of an experimental charge run at 11 GPa and 1050 °C (EM111). (a) Entire capsule with rectangle indicating the position of (b), a detailed view illustrating a magnesite crystal. Phase A and chondrodite are homogeneously distributed, but magnesite (mag) is typically adjacent to the diamond layer.

atmospheric CO_2 absorbed by brucite as mentioned above. A second possibility is oxidation of the diamond trap, and third, graphite deposition inside the capsule during arc welding from the graphite electrode.

The frequent appearance of magnesite at conditions >10 GPa, <1200 °C results from extremely small CO_2 solubilities in the fluid: Equilibrium calculations for a mixed CO_2–H_2O fluid, applying PerpleX (Connolly, 1990) and the Holland and Powell (1998) data base, yield molar CO_2 fractions in the fluid in equilibrium with magnesite of <0.00025. With our typical capsule size and amount of H_2O, this would lead to magnesite saturation with as little as 8 µg CO_2 in our experiments. In order to reduce CO_2 concentrations, extra steps were introduced during the sample preparation stage. Brucite was always fired at 120 °C in a vacuum furnace over night before use and every starting material was kept in the vacuum furnace before filling a capsule. We further employed silver instead of a graphite electrode during welding. These measures were successful in suppressing magnesite formation in our diamond-free experiments but despite taking the same precautions in this study, relatively big grains of magnesite still formed in some of the experiments. We thus infer that the diamond trap is indeed a carbon source and that the minor amount of magnesite forms through oxidation (easily achieved due to minor hydrogen loss through the capsule walls) of the diamond layer during the experiment.

3.2. Fluid/melt composition

Composition of fluids obtained from this experimental study are listed in Table 1 and illustrated in Figs. 3–5. The total amount of dissolved oxide components in the liquids increases from 20 to 42 to 58 wt% at 1000, 1200 and 1350 °C at 11 GPa (Fig. 3). At 13.5 GPa the amount of dissolved oxide components in the liquid increases only slightly from 40 to 47 wt% from 1100 to 1250 °C. Above 1100 °C the total amount of silicate in the liquid at 13.5 GPa is only a few wt% higher than at 11 GPa (Fig. 3a).

MgO/SiO_2 weight ratios generally decrease with increasing temperature (Fig. 3b) towards the bulk MgO/SiO_2 of 1.9. At the same temperature, MgO/SiO_2 ratios are lower at 13.5 than at 11.0 GPa. Unfortunately, errors are quite large (mostly due to the comparatively low SiO_2 concentrations), nevertheless, the following tendencies can be observed: At 13.5 GPa, MgO/SiO_2 weight ratios regularly

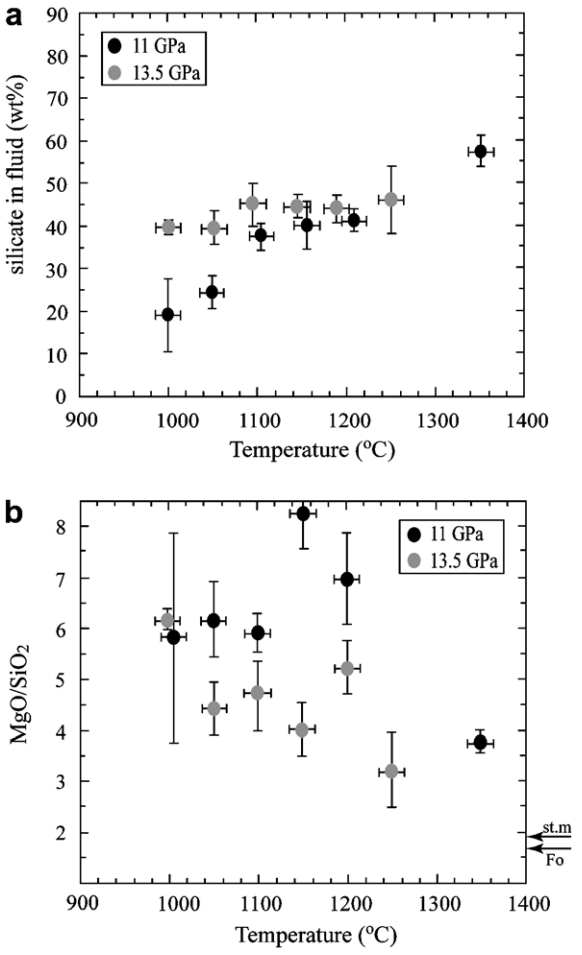

Fig. 3. (a) Temperature vs. total dissolved silicate-content in the fluid at 11 and 13.5 GPa. Note the increase of solute in the fluid at 11 GPa and the step of solute-content between 1050 and 1100 °C, both absent at 13.5 GPa. Error bars are 1σ. (b) MgO/SiO_2 weight ratios as a function of temperature. Ratios are decreasing with increasing temperature. Arrows show ratios for the starting material (st.m) and forsterite (Fo).

decrease from 6.2 (1000 °C) to 3.2 (1250 °C). At 11 GPa, MgO/SiO_2 weight ratios remain constant near 6 at 1000–1200 °C and then rapidly decrease to 3.8 at 1350 °C. Measurements at 1150 °C, 11 GPa resulted in an unrealistically high MgO/SiO_2 ratio of 8, due to comparatively low SiO_2-contents (Fig. 4a), which we cannot explain.

At 11 GPa an abrupt decrease in H_2O-content from 76 to 62 wt% is observed between 1050 and 1100 °C (Fig. 4a). After this step, H_2O-contents remain almost constant to 1200 °C, and then decrease at 1350 °C to 40 wt%. A similar behaviour is observed for the MgO and SiO_2 concentrations in the fluid. A step of 12 wt% in MgO is observed between 1050 and 1100 °C. From 1100 to 1200 °C, the concentration of MgO in the melt is about 35 wt% and then increases to 45 wt% at 1350 °C (Fig. 4a). A similar step in SiO_2 concentration between 1050 and 1100 °C is less apparent (Fig. 4a), as the absolute increase is small and amounts to about 2.1 wt%. However, this corresponds to a relative increase of 62% (Table 1). At 13.5 GPa, concentration steps in MgO and SiO_2 are smaller and there is a lesser increase of dissolved silicate in the fluid with temperature. Maximum concentration steps amount to 5 wt%, 1.5 wt% and 5.5 wt% for MgO, SiO_2 and H_2O, respectively (Fig. 4b), and are all within analytical error (Table 1). Due to the nearly continuous variations at 13.5 GPa we infer that the fluid–melt miscibility gap is closed at this pressure and that the liquid is supercritical with respect to the solidus endpoint. Fig. 5 summarizes liquid compositions in a ternary MSH diagram (in wt%) and shows the abrupt change in liquid composition between 1050 and 1100 °C at 11 GPa.

Our experimental results allow the definition of melting and dissolution reactions (Fig. 6) and the liquid volumes on the Mg-rich side of the MSH ternary at 11 and 13.5 GPa (Figs. 7 and 8). Our liquids mostly coexist with two solid phases (Table 1), and hence, these liquid compositions are buffered (solid circles in Figs. 7 and 8). The composition of liquids coexisting with enstatite and forsterite were added from Stalder et al. (2001) and Mibe et al. (2002). With increasing temperature, liquids become more silicate-rich and MgO/SiO_2 ratios decrease. Mass balance defines the 11 GPa melting reaction in compositions more magnesian than the tie-line forsterite–H_2O to

$$1.00(18)\ \text{phase A} + 1.07(4)\ \text{fluid} = 0.63 \pm (15)\ \text{chondrodite} + 1.44(2)\ \text{melt}$$

(in wt. proportions, 2σ errors obtained by Monte Carlo error propagation through mass balance calculation), leading to a melt with a MgO/SiO_2 wt-ratio almost identical to the subsolidus fluid (Fig. 3), but located to the MgO-side of tie-line phase A–fluid. The mineralogy of the solids coexisting with the liquid changes with increasing temperature at 11 GPa from phase A + clinohumite to phase A + chondrodite to chondrodite to forsterite + clinohumite. At 13.5 GPa the succession with increasing temperature is phase A + wadsleyite to phase A + clinohumite to superhydous B + forsterite to phase B + forsterite.

4. DISCUSSION

4.1. High-pressure melting for forsterite–enstatite–H_2O compositions

The composition of high-pressure melts in forsterite–enstatite–H_2O was investigated by Stalder et al. (2001) and Mibe et al. (2002). Fig. 9a shows all their constraints on liquid composition. Mibe et al. (2002) delimit liquid compositions at 1100 °C (3, 5, 8, and 10 GPa) and at 1250 °C at 5 GPa, Stalder et al. (2001) measured liquid compositions at 6 and 9 GPa, 900–1150 °C and at 10.5 GPa, 1150 °C. Typical pressure uncertainties in multi-anvil experiments are near 5%, therefore, we group data from 5 to 6 GPa, 8 to 9 GPa and 10 to 10.5 GPa of Mibe et al. (2002) and Stalder et al. (2001).

To explain the apparent disagreement at a given temperature between their and Stalder et al.'s (2001) data, Mibe et al. (2002) assumed that liquid in Stalder's experiments may not be pure H_2O but a diamond-saturated C–H–O

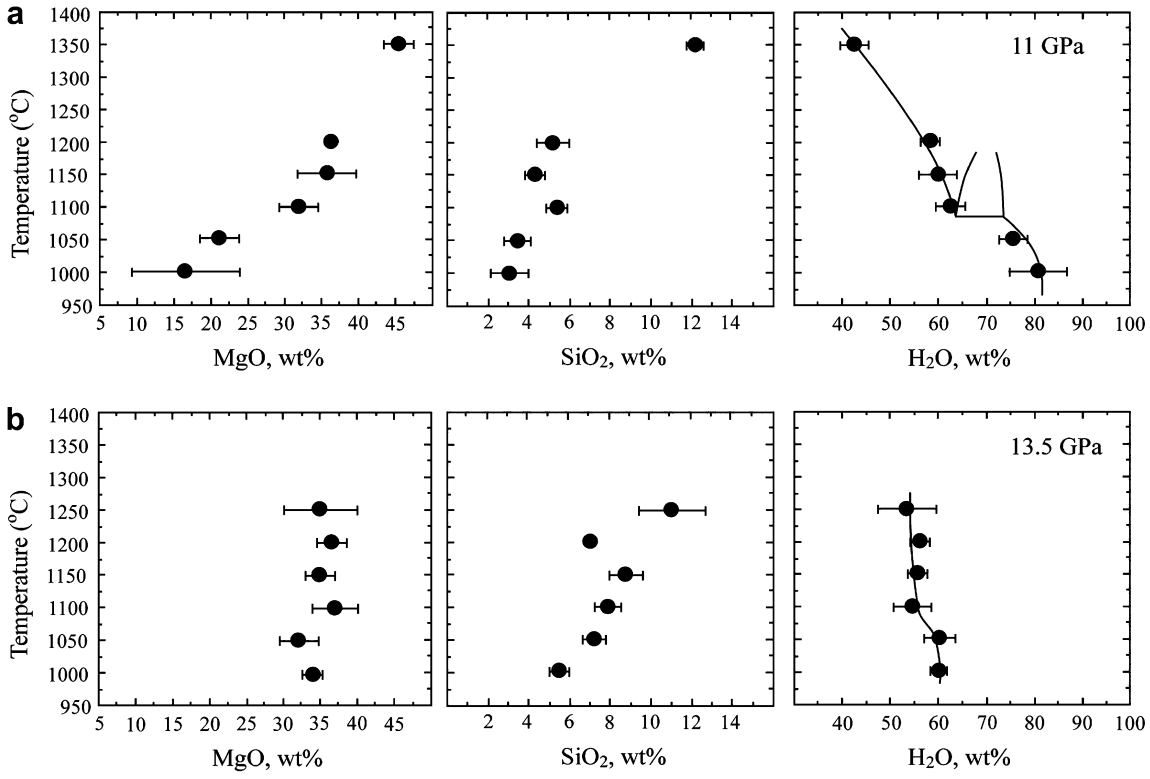

Fig. 4. MgO, SiO_2 and H_2O concentrations in the fluid vs. temperature for experimental liquids at (a) 11 GPa, and (b) 13.5 GPa. Variations of MgO, SiO_2 and H_2O in wt%. Error bars are 1σ. The lines in the right side diagrams indicate the interpretation of the data including a small melt–fluid miscibility gap at 11 GPa, but only a shoulder in the H_2O-contents of the fluid at 13.5 GPa.

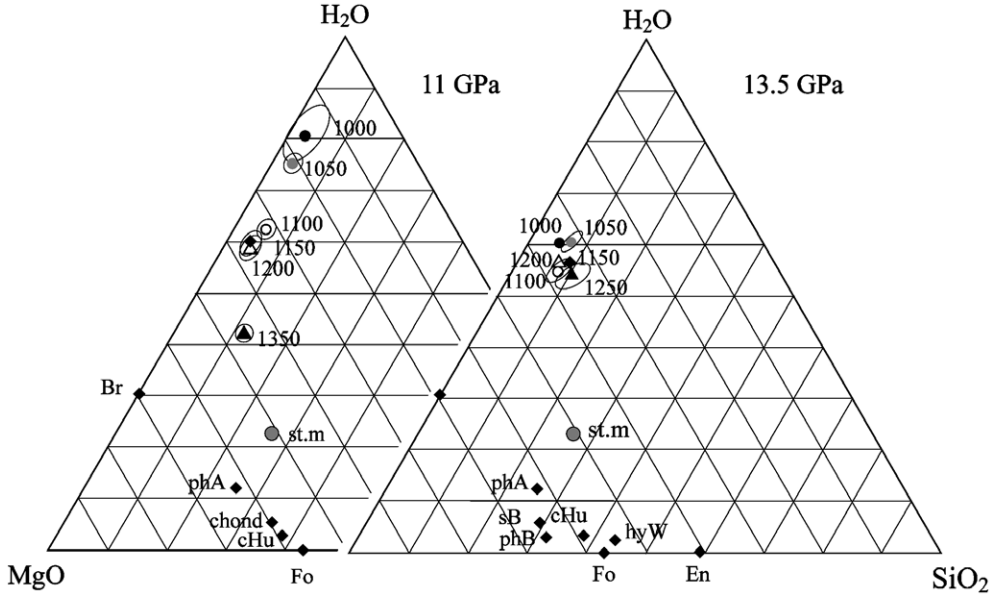

Fig. 5. Ternary MgO–SiO_2–H_2O diagram in wt% illustrating liquid compositions at 11 and 13.5 GPa. Numbers next to the symbols indicate temperatures (in °C). Symbol with abbreviation st.m locates the starting composition. Phase abbreviations are: phB, phase B; sB, superhydrous B; Br, brucite; cHu, clinohumite; chond, chondrodite; En, enstatite; Fo, forsterite; pha A, phase A; hyW, hydrous wadsleyite. An error ellipse is shown for each experiment. Where ellipses are absent, errors are smaller than symbol size.

liquid. However, the solidus temperature indicated by Stalder et al. (2001) was not shifted noticeably from the one determined by other studies in CO_2-free systems (Inoue, 1994; Irifune et al., 1998) arguing against significant CO_2 fractions in the fluid. Luth (1995), performed experiments in the MSH system and demonstrated that, with respect

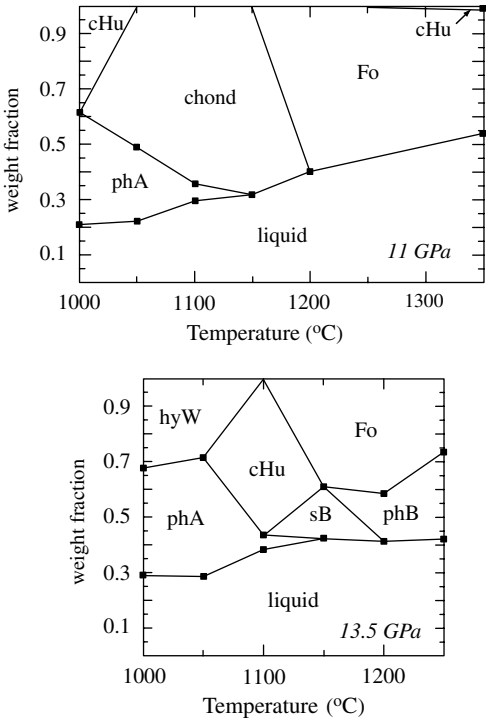

Fig. 6. Weight fraction of phases as a function of temperature for the given bulk composition. Abbreviations as in Fig. 5.

to a CO_2-free reaction, addition of carbonate does not significantly affect the position of the reaction phA + enstatite = forsterite + fluid, where the fluid is either purely aqueous or a mixed H_2O–CO_2 liquid.

Surprisingly, the simple interpretation that the solidus is at 1100 °C, at 5–10 GPa, is within the error of experimental temperatures, and consistent with all of the above data except for a single data point (Stalder et al.'s second fluid composition measurement at 1150 °C, 9 GPa): (i) Silicate solubilities of 55–60 wt% at 5 GPa, 1100–1250 °C, and of 65–75 wt% at 8 and 10 GPa, each at 1100 °C, reported by Mibe et al. (2002) are very similar to the silicate solubilities reported in Stalder et al. (2001) at 6, 9 (first experiment), and 10.5 GPa, 1150 °C, respectively (Fig. 9a). For each pressure, all results agree within experimental error. (ii) The results from Stalder et al. from 900 to 1100 °C define constantly increasing silicate-contents with temperature, from 5 to 15 wt% at 6 GPa and from 10 to 30 wt% at 9 GPa. At 1100 °C, silicate-contents in the Stalder liquids are 45 wt% lower than in the Mibe data. (iii) The two sets of experiments have employed different experimental setups, but typical temperature gradients of 20 °C in multi-anvil assemblages at 1100 °C allow the following consideration: if the effective temperature in the experiments at nominally 1100 °C was a few degrees lower for Stalder et al. and a few degrees higher for Mibe et al., then a solidus, across which H_2O-contents in the liquids increase by 40 wt%, can be placed at 1100 °C.

Concerning the inconsistent data point, Stalder et al. (2001) performed two experiments at 9 GPa, 1150 °C. One of them had a silicate concentration of 66 wt%, close to the 68 wt% found by Mibe et al. (2002) at 8 GPa, 1100 °C, but with a standard deviation of 57 wt%. This data point is shown in parenthesis in Fig. 9a. In a repeat experiment, the silicate concentration was 34 ± 10 wt%. The first experiments had run durations of 6 h, the latter of only 1 h. Stalder et al. (2001) preferred the result with 34 wt% of silicate in the liquid, and, thus, located the water-saturated solidus between 1100 and 1150 °C. Instead, accepting the other data point and dismissing the second because of its short duration, results in complete consistency of the two data sets.

Mibe et al. (2002) constrained liquid compositions in experiments at 1100 and 1250 °C. Thus, these experiments do not allow definition of a solidus present at lower temperatures. Nevertheless, Mibe et al.'s preferred value of 30 wt% silicate solubility in the liquid at 3 GPa (the experiments allow between 0 and 45 wt%), chosen by Mibe et al. to have the lowest possible MgO/SiO_2 ratio (see their Fig. 3), indi-

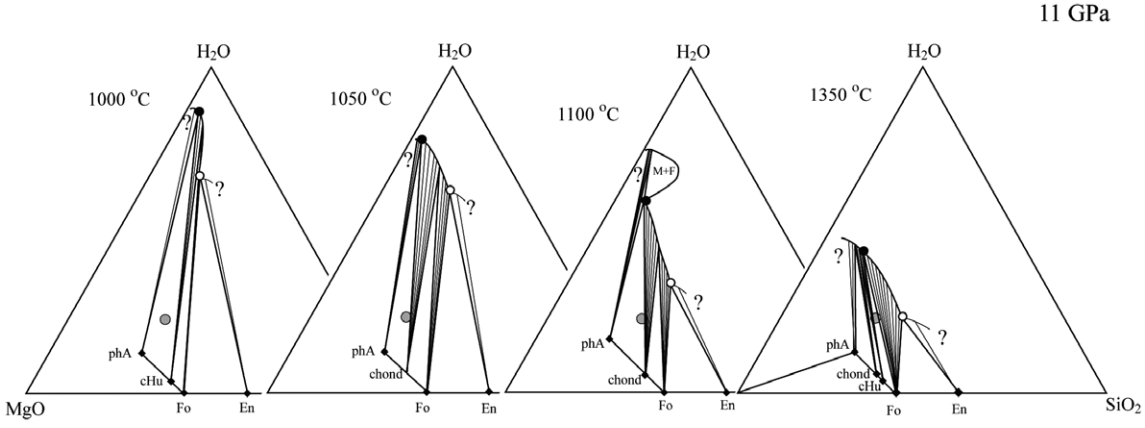

Fig. 7. Ternary diagrams (in wt%) illustrating the composition of hydrous fluid/melt at 11 GPa at 1000, 1050, 1100, and 1350 °C. MgO/SiO_2 ratios in fluids and melts coexisting with phase A, clinohumite, or chondrodite were obtained in this study (black circles), fluid/melt compositions coexisting with forsterite + enstatite are estimated from Stalder et al. (2001) and Mibe et al. (2002) (open circles). The large grey circle denotes the starting composition.

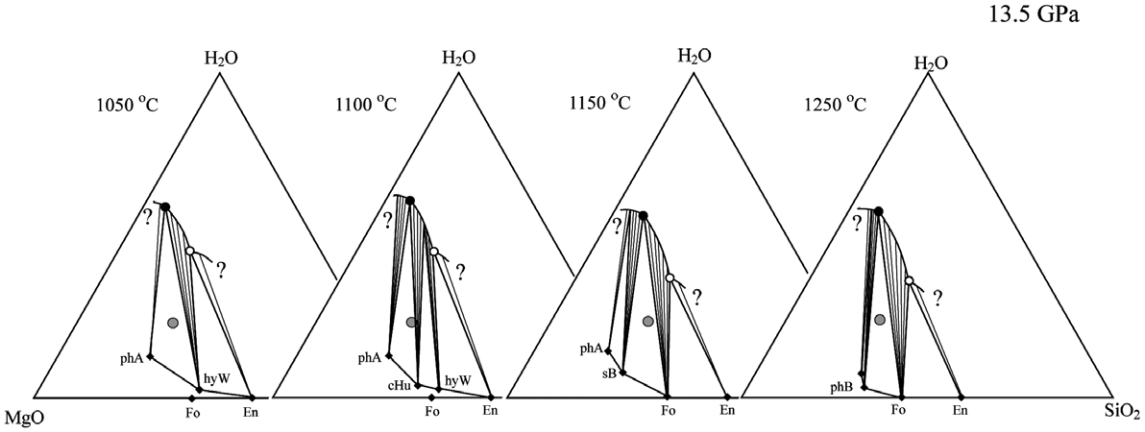

Fig. 8. Ternary diagrams (in wt%) illustrating the compositions of supercritical hydrous liquids at 13 GPa at 1050, 1100, 1150, and 1250 °C. MgO/SiO_2 ratios in fluids and melts were obtained in this study (black circles). Fluid/melt compositions coexisting with forsterite + enstatite are estimated (open circles). The large grey circle denotes the starting composition.

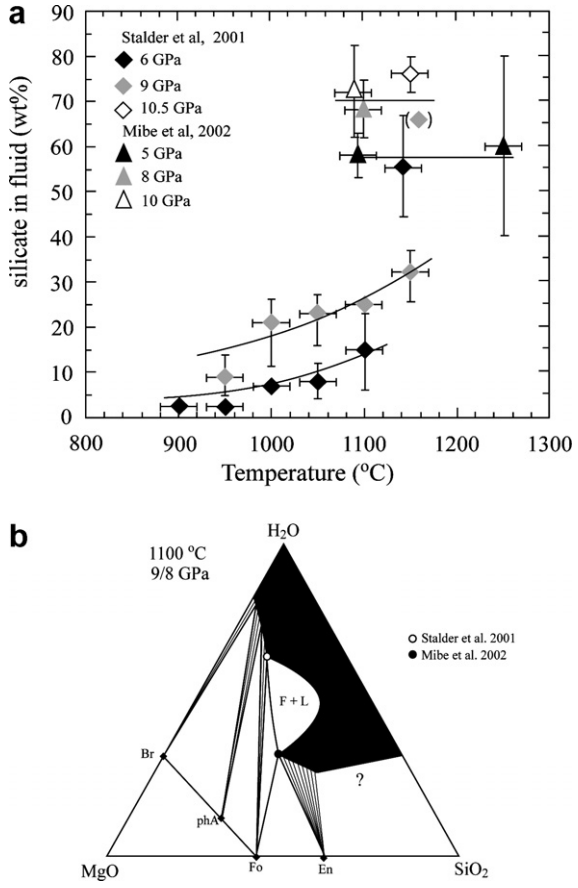

Fig. 9. (a) Total concentration of solutes in the liquid phases at 5, 6, 8, 9, 10 and 10.5 GPa from Mibe et al. (2002) and Stalder et al. (2001). (b) Ternary MSH (in wt%) diagram depicting the coexisting fluid, melt and solid phase compositions at 1100 °C and 8/9 GPa reconciling Mibe et al.'s (2002) and Stalder et al.'s (2001) data. The liquid volume boundaries are not well defined and understood as schematic.

cates that the solidus is overstepped in pressure between 3 and 5 GPa (the latter has 58 wt% silicate in the liquid).

We thus propose that the data set of Mibe et al. (2002) at 5–10 GPa and 1100 ± 20 °C are at supersolidus conditions while the Stalder et al. (2001) data set at 6–9 GPa and 1100 ± 20 °C was still at subsolidus conditions. Fig. 9b shows one possible interpretation of the data of the two groups at 8/9 GPa and 1100 °C. Similar to Mibe et al. (2002), our results indicate a solidus between 1050 and 1100 °C at 11 GPa. While Mibe's and Stalder's bulk compositions were within the triangle forsterite–enstatite–H_2O, our bulk was in the triangle forsterite–phase A–H_2O, i.e., to the Mg-rich side of the tie-line forsterite–H_2O. As will be shown below, our solidus should be at slightly higher temperatures than the one in the forsterite–enstatite–H_2O bulk system. Stalder et al.'s and our results were obtained in the same laboratory but with different experimental set-ups (different octahedron size and assemblage, thermocouple changed from S- to B-type, slightly different placement of thermocouple), and again we ascribe the small differences to the imprecision of absolute temperatures in multi-anvil experiments.

4.2. A compilation of the MSH solidi

Fig. 10 compiles solidi determined in H_2O-saturated MSH systems and in natural peridotite. Kushiro and coworkers (Kushiro et al., 1968b; Kushiro, 1969; Kushiro and Yoder, 1969; Nakamura and Kushiro, 1974) defined melting relations of forsterite + H_2O and enstatite + H_2O to 3 GPa, and Inoue (1994) from 5 to 12 GPa.

Up to a pressure of about 4.5 GPa, equilibration of enstatite + H_2O result in enstatite + forsterite + fluid at subsolidus conditions, enstatite + fluid melt incongruently near 1200 °C producing forsterite + melt (Kushiro et al., 1968b). This result is consistent with fluids having an MgO/SiO_2 weight ratio smaller than enstatite at <3.0 GPa, 1000 °C and < 5 GPa, 1200 °C (Newton and Manning, 2002; Kawamoto et al., 2004). Between 4.5 and 13.5 GPa enstatite dissolves or melts congruently (Inoue,

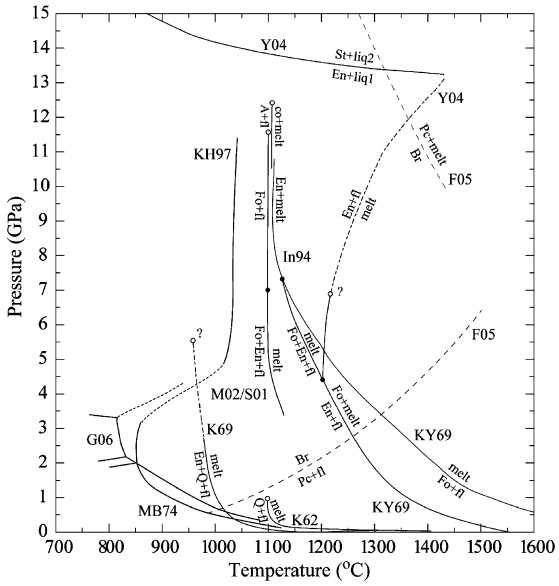

Fig. 10. Pressure–temperature diagram compiling solidus curves and second critical endpoints for various subsystems in the MSH ternary and for natural peridotite compositions. Note that MSH peridotite melting is incongruent for enstatite + fluid at low pressures and for forsterite + fluid at high pressures, but that melting is eutectic for enstatite + forsterite + fluid at intermediate pressures. The solidus temperature depression for natural peridotite (G06, MB74, and KH97) is a result from the presence of the additional Al, and Na–Ca phases. The changes in slope of the natural peridotite solidi correspond to a change in the stable Al-phase (spinel and garnet for MB74, spinel, chlorite, and garnet for G06). The strong temperature increase above 3 GPa is likely to result from a change from an incompatible to a compatible behaviour of sodium in clinopyroxene. Note that the eutectic enstatite + quartz + fluid reaction is only defined at 2 GPa and at atmospheric pressure. The endpoints of the enstatite + quartz + fluid and enstatite + fluid melting reactions are unknown. Here they are placed to respect the sequence $P_{(qz+fluid)} < P_{(en+qz+fluid)} < P_{(en+fluid)} < P_{(fo+fluid)} < P_{(A+fluid)}$, where the parenthesis denotes the low temperature side of each solidus. Sources: F05, (Fukui et al., 2005); G06, Grove et al. (2006); In94, Inoue (1994); K62, Kennedy et al. (1962); K69, Kushiro (1969); KH97, Kawamoto and Holloway (1997); KY69, Kushiro and Yoder (1969); M02/S01, Mibe et al. (2002) and Stalder et al. (2001); MB74, Mysen and Boettcher (1974); Y04, Yamada et al. (2004). A, phase A; co, chondrodite; Q, quartz; and other abbreviations as in Fig. 5.

1994; Yamada et al., 2004). Additionally, Yamada et al. (2004) based on textural arguments infer that the (congruent) melting reaction of enstatite + H_2O reaches to 13 GPa, 1450 ± 50 °C. Above 13.5 GPa, equilibration of enstatite + H_2O results in enstatite + stishovite + liquid, liquids thus have a MgO/SiO_2 weight ratio larger than enstatite. The latter observation is unequivocal and independent of the nature of the liquid phase. However, the persistence of a wet enstatite solidus to 13.5 GPa would imply that the thermal barrier located at the enstatite–fluid tie-line separating eutectics or peritectics on both sides of this fluid tie-line persists up to 13.5 GPa and that the enstatite + fluid solidus evolves to a temperature 300 °C higher than that of forsterite + fluid. This aspect is not yet fully clarified and should be reinvestigated using a technique measuring the composition of the liquid phase coexisting with enstatite in the pseudobinary enstatite – H_2O to demonstrate the discontinuous nature and composition of the liquid phase.

Forsterite exhibits a behaviour opposite to enstatite: at low pressures dissolution and melting of forsterite + H_2O are congruent at near melting temperatures, while at pressures around 7.7 GPa, melting becomes incongruent resulting in enstatite + melt (Inoue, 1994). At >7.7 GPa, melts thus have MgO/SiO_2 wt-ratios >1.34. Stalder et al. (2001) determine the MgO/SiO_2 wt-ratio in the melt to 0.95–1.5 at 6 GPa, 1.35–1.6 at 9 GPa, and 1.4 at 10.5 GPa, consistent with the above result. Mibe et al. (2002) bracketed this ratio at 1100 °C, 5 and 8 GPa, to 1.06–1.21; at 10 GPa, the MgO/SiO_2 ratio was determined to be ~1.4. While the 5 and 10 GPa MgO/SiO_2-ratios are consistent with the above results, the 8 GPa ratio is not. However, overlooking a small amount of enstatite, possibly concentrated in a corner of the capsule that was not investigated, in this one critical experiment at 8 GPa by Mibe et al. would yield consistency, allowing for more magnesian liquids. Fluid compositions in equilibrium with enstatite and forsterite yielded MgO/SiO_2 ratios <0.67 at 900–1200 °C, 1–2 GPa (Zhang and Frantz, 2000) and an MgO/SiO_2-ratio ⩾0.67 at 3 GPa, 1100 °C (Stalder et al., 2001; Mibe et al., 2002; Kawamoto et al., 2004) confirming incongruent dissolution of enstatite + H_2O at these pressures.

From the incongruent melting of enstatite below 4.5 GPa, and the incongruent melting of forsterite above ca. 7.7 GPa, it follows, that between 4.5 and 7.7 GPa melt compositions in equilibrium with forsterite and enstatite must have Mg/Si ratios between those of forsterite and enstatite. Thus, the melting of forsterite + enstatite + H_2O is eutectic in this pressure range, as drawn in Fig. 11.

Remarkably, all available data (Inoue, 1994; Stalder et al., 2001; Mibe et al., 2002) are consistent with a forsterite + enstatite + H_2O melting temperature near 1100 °C above 7 GPa. This compares to a near constant melting temperature of 1000 °C for hydrous natural peridotite at 5–11 GPa (Kawamoto and Holloway, 1997). Stalder et al. (2001) speculated that the endpoint of this solidus in the $MgO–SiO_2–H_2O$ system should be located around 12–13 GPa. Our data in a more magnesian phase A–forsterite–H_2O composition indicate an endpoint between 11 and 13.5 GPa, just below 1100 °C. This latter solidus as well as its critical endpoint must be located, at slightly higher pressure and temperature than in the peridotite model system forsterite + enstatite + H_2O (see below).

In a recent article, (Mibe et al., 2007) describe multi-anvil experiments in a peridotite–H_2O system in which they observe, through in-situ X-ray imaging on a synchrotron, two coexisting liquids between 1.7 GPa, 1000 °C and 3.6 GPa, 1190 °C. At 4 GPa and 1240 °C two liquids could not be distinguished, which is interpreted as the closure of the fluid–melt immiscibility gap. This interpretation is at odds with all previous studies on peridotites and their simple MSH subsystem in the pressure–temperature region concerned. Careful examination of the experimental results of Mibe et al. (2007) reveals that their interpretation of hav-

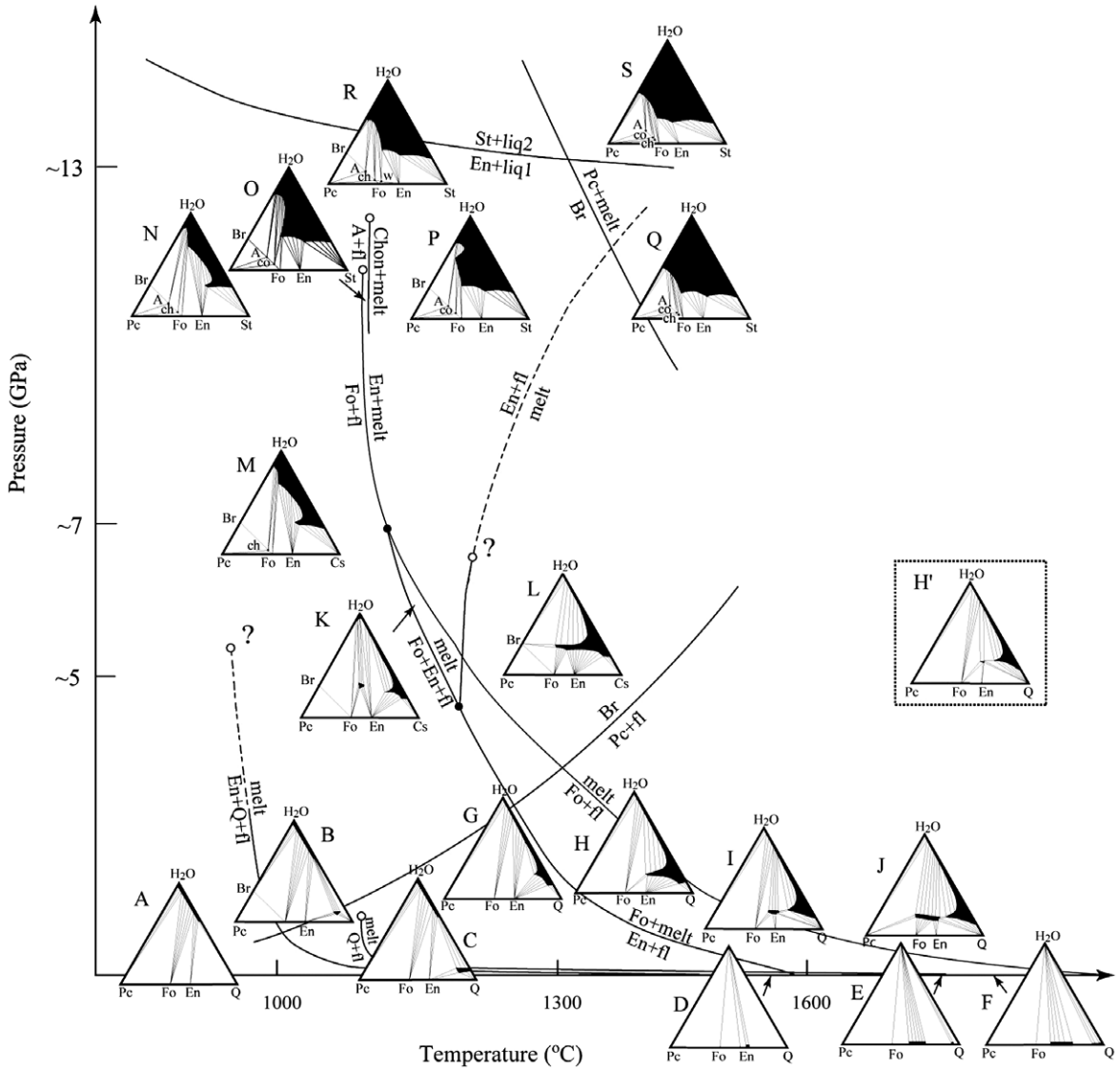

Fig. 11. Schematic pressure–temperature diagram indicating solidus curves and second critical endpoints for various subsystems in the MSH ternary (see Fig. 10) with chemographies and the topologies of the liquid volumes. At atmospheric pressures and high temperatures, two silicate melts coexist; the pressure to which this miscibility gap remains open is unknown. Supercriticality with respect to the solidi begins at the endpoint of the quartz + fluid = melt reaction at the Si-rich side of the diagram. In our interpretation, the supercritical liquid volume evolves to the Mg-rich side with pressure, until finally compositions more magnesian than forsterite become supercritical as defined in this study. The open circles with an adjacent question mark indicate possible endpoint positions for the solidi of enstatite + quartz + fluid and for enstatite + fluid. Liquid 1 refers to a liquid with a MgO/SiO_2 ratio identical to enstatite, while at higher pressures, liquid 2 has a MgO/SiO_2 ratio higher than enstatite. A, phase A; ch, clinohumite; co, chondrodite; and other abbreviations as in Fig. 5. For discussion and data sources see text.

ing achieved conditions above the closure of the fluid–melt immiscibility gap are in fact not supported by their data.

First, all but two experiments of Mibe et al. (2007) are at bulk H_2O-contents of 55–63 wt%. The experiments, where the solid products were investigated by Mibe et al. (2007), contained an undetermined amount of olivine. The presence of 10–20% of olivine (the images of Mibe et al. suggest higher amounts) would increase the H_2O-content of the liquids proportionally, and place the experimental liquids of Mibe et al. (2007) at 65–80% H_2O. Such liquid would be at the fluid side of the fluid–melt immiscibility gap at the investigated temperatures and pressures. Consequently it is not surprising, that two liquid phases could not be detected in these experiments. Thus, these experiments do not constrain the critical point of the fluid–melt immiscibility gap.

Second, the method of observing two phases through X-ray imaging is critically dependent on the X-ray contrast between the two phases. However, the discernible X-ray contrast is not indicated in Mibe et al. (2007) and hence it is unknown to what extend the narrowing of the immiscibility gap could be theoretically observed, and at which width two coexisting liquids would become indistinguishable.

Third, the two experiments performed at lower H_2O-contents at 4 GPa, i.e., at 22 and at 40 wt% both contained olivine and orthopyroxene. The persistence of orthopyroxene in a peridotite bulk composition indicates >50% of crystals to be present in these experiments. Again the liquid H_2O-content would be much higher than the bulk H_2O-content, but more critical, the capsule would be mostly filled by a solid grain matrix with intergranular space occupied by one or two liquids. Under these circumstances, the two liquids are unlikely to separate into large bubbles (which is necessary to be distinguished by this method). Furthermore, the largest X-ray contrast would be between the solid minerals and the liquid phase(s). Mibe et al. state, that under the investigated conditions they cannot distinguish the solids separately. The two liquids having a comparatively smaller X-ray contrast, in particular when the immiscibility gap narrows, are thus unlikely to be distinguishable within a solid grain matrix. We conclude that the observations by Mibe et al. do not constrain the critical point of the fluid–melt miscibility gap at any of the investigated conditions and thus also not the position of the endpoint of the solidus in the peridotite system.

4.3. The MgO–SiO_2–H_2O phase diagram and ternary chemographies: the evolution of the liquid volume with pressure and temperature

The existing experiments into the MSH system at near or above solidus temperatures can be compiled to delineate the evolution of the liquid volume in the model mantle system with pressure and temperature. Although information is incomplete, the topology of the liquid volume is constrained for all but two areas of the pressure–temperature space of interest.

Melting in the system starts with the enstatite + quartz + fluid eutectic at 975 °C (investigated at 2 GPa by Kushiro, 1969, chemography A to B in Fig. 11) and is followed by the equilibrium quartz + fluid = melt (B to C, Fig. 11). The latter terminates in a critical endpoint at 1080 °C, 0.97 GPa (Kennedy et al., 1962, C to G, Fig. 11), while the critical endpoint of enstatite + quartz + fluid = melt is unknown. At higher temperatures but ambient pressure, the minimum melting in MgO–SiO_2 is eutectic between enstatite and quartz, and immiscibility of two silicate melts occurs for compositions between enstatite and quartz from 1687 to ~2200 °C (D–F, Fig. 11, Ol'shanskii, 1951; Wu et al., 1993 and references therein). In the dry system the two melt immiscibility remains to pressures of 1.5 GPa (Hudon et al., 2004) but has vanished at 5 GPa (Dalton and Presnall, 1997) due to the strong temperature increase of the dry quartz/coesite melting reaction with pressure, rendering the immiscibility gap metastable. Addition of H_2O strongly suppresses the quartz/coesite melting temperature but probably has only a small influence on the miscibility gap. It can thus be inferred that the immiscibility gap extends to at least similar pressures in the H_2O-bearing than in the dry system (I and J, Fig. 11), but its width and critical pressure are unknown.

At 1.5 GPa, the liquid volume in the MSH system was outlined by Kushiro et al. (1968a) between 1280 and 1340 °C (G and H, Fig. 11). Although a continuous melt region is drawn by Kushiro et al. (1968a) and in chemography H of Fig. 11, the data of Kushiro would also permit two coexisting silicate melts at temperatures above the peritectic reaction enstatite + fluid = forsterite + melt, i.e., at 1.5 GPa, 1340 °C. Chemography H or H′ in Fig. 11 would be alternative possibilities.

At intermediate pressures (e.g., 5 GPa), the experimental data allow two alternative topologies: Either two eutectics, one located in the forsterite–enstatite–fluid subsystem, the other in the enstatite–quartz–fluid subsystem, or one eutectic in the forsterite–enstatite–fluid subsystem but an already supercritical behaviour of the enstatite–quartz–H_2O subsystem (as mentioned above, the pressure of the endpoint to the reaction enstatite + quartz + fluid = melt is unknown). In both cases, this results in two separate liquid volumes (K in Fig. 11), similar to the situation in the dry forsterite–quartz system at 0.2–2.5 GPa (Chen and Presnall, 1975). The two melt volumes are separated by the enstatite–fluid tie-lines and thus critically depend on the enstatite + H_2O melting temperature. This latter temperature is higher than the enstatite + quartz + H_2O and the forsterite + enstatite + H_2O melting reactions at pressures above 4.5 GPa. To pressures at which the enstatite–fluid tie-line exists, the two melt volumes to the forsterite and quartz sides of the tie-line remain separated. At higher pressures, these two melt volumes would join and the melt volume extend more and more to the magnesian side (P, Fig. 11).

The reaction enstatite + fluid = melt was determined on textural arguments (Inoue, 1994 and Yamada et al., 2004), a method that is not reliable when silicate solubilities in the aqueous fluid become similar to those of melts. A simple interpretation of phase relations in MSH, keeping the above separated liquid volumes to a minimum, is only possible when this melting reaction ends at significantly lower pressure than inferred by Inoue (1994) and Yamada et al. (2004). Furthermore, it is likely, that the fluid–melt miscibility gap for an enstatite + H_2O composition closes at lower pressures than for the forsterite + H_2O system: the lowest solidus endpoint occurs on the SiO_2–H_2O join, and liquid volumes grow with increasing pressure from the SiO_2–H_2O side towards more magnesian compositions. In our interpretation (Fig. 11), we thus place the relative pressures of the critical endpoints of the MSH solidi in the sequence $P_{(qz+fluid)} < P_{(en+qz+fluid)} < P_{(en+fluid)} < P_{(fo+fluid)} < P_{(A+fluid)}$, where the parenthesis denotes the low temperature side of each solidus. This has to be experimentally confirmed, and the area between chemographies L, M, and P remains the least constrained.

We infer that the enstatite + fluid melting reaction has an endpoint at intermediate pressures, i.e., between that of quartz + fluid and forsterite + fluid, leading to complete fluid–melt miscibility for compositions in enstatite–coesite–H_2O at pressures lower than the endpoint of the forsterite + fluid melting reaction (Si-rich portion of O, P, and Q, Fig. 11). This interpretation is strengthened by the observation of Yamada et al. (2004), that enstatite + H_2O compositions produce stishovite + melt at >14 GPa, i.e., enstatite dissolves again incongruently but this time producing stishovite and a MgO-rich liquid. The incongruent

dissolution occurs at 300 °C lower temperatures than the supposed enstatite + fluid = melt reaction, which is difficult to understand without a continuous single melt field at such pressures (see Fig. 11, P to S or Q to S).

At the pressures of this study, the endpoints of the forsterite + fluid and the phase A + fluid melting reactions are located as discussed above, i.e., the melting reaction on forsterite + fluid at slightly lower temperatures than that of phase A + fluid. Chemographies N to P and R depict this topology and are equivalent to those in Figs. 6–8.

With pressure, the dissolution and melting reactions of enstatite + H_2O thus change from incongruent and forsterite producing, to congruent, and than to incongruent and stishovite producing, liquids becoming increasingly magnesian with pressure. Similarly, forsterite melts congruently at low pressures but incongruently and enstatite producing at higher pressures, the involved melts becoming again more magnesian with pressure. The continuous evolution of liquids towards more magnesian compositions, as already proposed by Stalder et al. (2001) and Mibe et al. (2002), indicates that the fluid–melt immiscibility gap closes from the Si-rich to the Mg-rich side with increasing pressure, making the Mg-rich side investigated in this study the portion of $MgO–SiO_2–H_2O$ space at which the solidus reaction should disappear at the highest pressure (setting aside the unknown relation on the $MgO–H_2O$ join).

5. CONCLUSIONS

Our measurements define a discontinuous evolution of liquid composition near 1100 °C, 11 GPa, that we interpret as a solidus reaction. At 13.5 GPa, this discontinuity is not present anymore, indicating that the critical endpoint of the solidus has been overstepped in pressure and that the $MgO–SiO_2–H_2O$ system contains only one supercritical liquid—with the exception of possibly two liquids coexisting on the $MgO–H_2O$ join. These results agree with Stalder et al.'s (2001) interpretation and Mibe et al.'s (2002) data that the rapid change in MgO and SiO_2 concentrations in the liquid at 1100 °C, 6 and 9 GPa, are evidence for the existence of an immiscibility gap. Our and Stalder's techniques can only constrain liquid compositions at the solidus, but not the existence and compositions of two coexisting liquids. In this sense, the critical curves of the MSH system remain unknown.

As outlined above, for a complete interpretation of the MSH liquid volume, a determination of H_2O-contents in the liquids coexisting with enstatite-only would be critical. This is necessary to understand at which conditions the two separate liquid volumes (at intermediate pressures, Fig. 11) become a continuous surface.

Previous results between 1 and 10.5 GPa (e.g., Nakamura and Kushiro, 1974; Yamamoto and Akimoto, 1977; Ryabchikov et al., 1982) showed that in the forsterite–quartz–H_2O subsystem of the MSH ternary, fluid compositions shift with increasing pressure to the MgO-rich side and solid residuals becomes enriched in silica. Our study demonstrates that this trend continues to more magnesian bulk compositions. As a consequence of the Mg-rich nature of our starting material, considerably more MgO and comparatively less SiO_2 are dissolved in the fluid phase resulting in MgO/SiO_2 weight ratios higher than for forsterite. It is unlikely to obtain such fluids with MgO/SiO_2 weight ratios between 6 and 4 in equilibrium with harzburgitic or lherzolitic mantle, but in dunites and olivine dominated such fluids might occur and further metasomatize the mantle at high pressures.

Our results supplement previous investigations from studies conducted at lower MgO/SiO_2 ratios and allow the understanding and modelling of solid parageneses, fluids, and melts in highly magnesian compositions. Regarding the many, but still only partly known, solidus endpoints, they provide the missing link to understand the supercritical nature of liquids in the entire $MgO–SiO_2–H_2O$ system which in turn provides the bases for the principal understanding of fluid–solid interaction and metasomatism mantle systems.

ACKNOWLEDGMENTS

We thank A. Hack and M. Aerts for their helpful discussions and advice, C. Manning and T. Kawamoto for constructive reviews, and finally A.J. Teague for improving the English. This study was supported from ETH research Grant 39/02-1.

REFERENCES

Chen C. H., and Presnall D. C. (1975) System Mg_2SiO_4-SiO_2 at pressures up to 25 kilobars. *Am. Mineral.* **60**(5–6), 398–406.

Connolly J. A. D. (1990) Multivatiable phase-diagrams-an algorithm based on generalized thermodynamics. *Am. J. Sci.* **290**(6), 666–718.

Dalton J. A., and Presnall D. C. (1997) No liquid immiscibility in the system $MgSiO_3–SiO_2$ at 5.0 GPa. *Geochem. Cosmochim. Acta* **61**(12), 2367–2373.

Fukui H., Inoue T., Yasui T., Katsura T., Funakoshi K., and Ohtaka O. (2005) Decomposition of brucite up to 20 GPa: evidence for high MgO-solubility in the liquid phase. *Eur. J. Mineral.* **17**(2), 261–267.

Grove T. L., Chatterjee N., Parman S. W., and Medard E. (2006) The influence of H_2O on mantle wedge melting. *Earth. Planet. Sc. Lett.* **249**, 74–89.

Gunther D., Frischknecht R., Heinrich C. A., and Kahlert H. J. (1997) Capabilities of an Argon Fluoride 193 nm excimer laser for laser ablation inductively coupled plasma mass spectrometry microanalysis of geological materials. *J. Anal. Atom. Spectrom.* **12**(9), 939–944.

Holland T., and Powell R. (1998) An internally consistent thermodynamic data set for phases of petrological interest. *J. Met. Geol.* **16**(3), 309–343.

Holzapfel W. B., and Franck E. U. (1966) Conductance and ion dissociation of water up to 1000 °C and 100 kilo bars. *Ber. Bunsenges. Phys. Chem.* **70**(9–10), 1105–1112.

Hudon P., Jung I. H., and Baker D. R. (2004) Effect of pressure on liquid–liquid miscibility gaps: a case study of the systems $CaO–SiO_2$, $MgO–SiO_2$, and $CaMgSi_2O_6–SiO_2$. *J. Geophys. Res.* **109**, 1–18.

Inoue T. (1994) Effect of water on melting phase-relations and melt composition in the system $Mg_2SiO_4–MgSiO_3–H_2O$ up to15 GPa. *Phys. Earth Planet. Inter.* **85**, 237–263.

Irifune T., Kubo N., Isshiki M., and Yamasaki Y. (1998) Phase transformations in serpentine and transportation of water into the lower mantle. *Geophys. Res. Lett.* **25**, 203–206.

Kawamoto T., and Holloway J. R. (1997) Melting temperature and partial melt chemistry of H_2O-saturated mantle peridotite to 11 gigapascals. *Science* **276**, 240–243.

Kawamoto T., Matsukage K. N., Mibe K., Isshiki M., Nishimura K., Ishimatsu N., and Ono S. (2004) Mg/Si ratios of aqueous fluids coexisting with forsterite and enstatite based on the phase relations in the Mg_2SiO_4–SiO_2–H_2O system. *Am. Mineral.* **89**(10), 1433–1437.

Kennedy G. C., Heard H. C., Wasserburg G. J., and Newton R. C. (1962) Upper 3-phase region in system SiO_2–H_2O. *Am. J. Sci.* **260**(7), 501–521.

Kessel R., Schmidt M. W., Ulmer P., and Pettke T. (2005a) Trace element signature of subduction-zone fluids, melts and supercritical liquids at 120–180 km depth. *Nature* **437**, 724–727.

Kessel R., Ulmer P., Pettke T., and Schmidt M. W. (2005b) The water-basalt system at 4 to 6 GPa: phase relations and second critical endpoint in a K-free eclogite at 700 to 1400 °C Earth Planet. *Sci. Lett.* **237**(3–4), 873–892.

Kessel R., Ulmer P., Pettke T., Schmidt M. W., and Thompson A. B. (2004) A novel approach to determine high-pressure high-temperature fluid and melt compositions using diamond-trap experiments. *Am. Mineral.* **89**(7), 1078–1086.

Komabayashi T., and Omori S. (2006) Internally consistent thermodynamic data set for dense hydrous magnesium silicates up to 35 GPa, 1600 °C: implications for circulation in the Earth's deep mantle. *Phys. Earth Planet. Inter.* **156**, 89–107.

Kushiro I. (1969) System forsterite–diopside–silica with and without water at high pressures. *Am. J. Sci.* **267**, 269.

Kushiro I., Syono Y., and Akimoto S. I. (1968a) Melting of a peridotite nodule at high pressures and high water pressure. *J. Geophys. Res.* **73**(18), 6023-&.

Kushiro I., and Yoder H. S. (1969) Melting of forsterite and enstatite at high pressures under hydrous conditions. *Carn. Inst. Wash. Year Book* **67**, 153–158.

Kushiro I., Yoder H. S., and Nishikawa M. (1968b) Effect of water on melting of enstatite. *Geol. Soc. Am. Bull.* **79**(12), 1685-&.

Longerich H. P., Jackson S. E., and Gunther D. (1996) Laser ablation inductively coupled plasma mass spectrometric transient signal data acquisition and analyte concentration calculation. *J. Anal. Atom. Spectrom.* **11**(9), 899–904.

Luth R. W. (1995) Is phase-A relavent to the earth mantle? *Geochem. Cosmochim. Acta* **59**(4), 679–682.

Manning C. (2004) The chemistry of subduction-zone fluids. *Earth Planet. Sci. Lett.* **223**(1–2), 1–16.

Mibe K., Fujii T., and Yasuda A. (2002) Composition of aqueous fluid coexisting with mantle minerals at high pressure and its bearing on the differentiation of the Earth's mantle Geochim. *Cosmochim. Acta* **66**(12), 2273–2285.

Mibe K., Fujii T., and Yasuda A. (2004) Response to the comment by R. Stalder on "Composition of aqueous fluid coexisting with mantle minerals at high pressure and its bearing on the differentiation of the Earth's mantle". *Geochim. Cosmochim. Acta* **68**(4), 929–930.

Mibe K., Kanzaki M., Kawamoto T., Matsukage K. N., Fei Y., and Ono S. (2007) Second critical endpoint in the peridotite–H_2O system. *J. Geophys. Res.* **112**, B03201. doi:10.1029/2005JB004125.

Morishima H., Kato T., Suto M., Ohtani E., Urakawa S., Utsumi W., Shimomura O., and Kikegawa T. (1994) The phase-boundary between alpha-Mg_2SiO_4 and beta-Mg_2SiO_4 determined by in-situ X-ray-observation. *Science* **265**(5176), 1202–1203.

Mysen B. O., and Boettcher A. L. (1974) Melting of a hydrous mantle: I. Phase relations of natural peridotite at high pressures and temperatures with controlled activities of water, carbon dioxide, and hydrogen. *J. Petrol.* **16**, 520–548.

Nakamura Y., and Kushiro I. (1974) Composition of gas phase in Mg_2SiO_4–SiO_2–H_2O at 15 kbar. *Carn. Inst. Wash. Year Book* **73**, 255–258.

Newton R. C., and Manning C. E. (2002) Solubility of enstatite plus forsterite in H_2O at deep crust/upper mantle conditions: 4 to 15 kbar and 700 to 900 °C. *Geochem. Cosmochim. Acta* **66**(23), 4165–4176.

Ol'shanskii Y. I. (1951) Equilibrium of two immiscible liquids in silicate systems of alkali-earth metals. *Doklady Akademii Nauk SSSR* **76**(1), 93–96.

Paillat O., Elphick S. C., and Brown W. L. (1992) The solubility of water in NaAlSi3O8 melts: a re-examination of Ab–H_2O phase relationships and critical behaviour at high pressures. *Contrib. Mineral. Petrol.* **1992**(112), 490–500.

Pettke T., Halter W. E., Webster J. D., Aigner-Torres M., and Heinrich C. A. (2004) Accurate quantification of melt inclusion chemistry by LA-ICPMS: a comparison with EMP and SIMS and advantages and possible limitations of these methods. *Lithos* **78**(4), 333–361.

Ryabchikov I. D., Schreyer W., and Abraham K. (1982) Composition of aqueous fluids in equlibrium with pyroxenes and olivines at mantle pressures and temperatures. *Contrib. Mineral. Petrol.* **79**(1), 80–84.

Schmidt M. W., and Ulmer P. (2004) A rocking multianvil: elimination of chemical segregation in fluid-saturated high-pressure experiments. *Geochim. Cosmochim. Acta* **68**(8), 1889–1899.

Stalder R., and Ulmer P. (2004) Comment on K. Mibe, T. Fujii, and A. Yasuda (2002), "Composition of aqueous fluid coexisting with mantle minerals at high pressure and its bearing on the differentiation of the Earth's mantle," Geochem. Cosmochim. Acta 66, 2273–2285. *Geochim. Cosmochim. Acta* **68**(4).

Stalder R., Ulmer P., Thompson A. B., and Gunther D. (2000) Experimental approach to constrain second critical end points in fluid/silicate systems: near-solidus fluids and melts in the system albite–H_2O. *Am. Mineral.* **85**(1), 68–77.

Stalder R., Ulmer P., Thompson A. B., and Gunther D. (2001) High pressure fluids in the system MgO–SiO_2–H_2O under upper mantle conditions. *Contrib. Mineral. Petrol.* **140**(5), 607–618.

Wu P., Eriksson G., Pelton A. D., and Blander M. (1993) Prediction of the thermodynamic properties and phase-diagrams of silicate systems-evaluation of the FeO–MgO–SiO_2 system. *ISIJ Int.* **33**(1), 26–35.

Yagi T., and Akimoto S. I. (1976) Direct determination of coesite-stishovite transition by insitu X-ray measurements. *Tectonophysics* **35**(1–3), 259–270.

Yamada A., Inoue T., and Irifune T. (2004) Melting of enstatite from 13 to 18 GPa under hydrous conditions. *Phys. Earth Planet. Inter.* **147**, 45–56.

Yamamoto K., and Akimoto S. (1977) System MgO–SiO_2–H_2O at high-pressure and temperature-stability field hydroxyl-chondrodite, hydroxyl-clinohumite and 10 A-phase. *Am. J. Sci.* **277**(3), 288–312.

Zhang J., Li B., Utsumi W., and Liebermann R. C. (1996) In situ X-ray observation of the coesite–stishovite transition: reversed phase boundary and kinetics. *Phys. Chem. Mineral.* **23**, 1–10.

Zhang Y. G., and Frantz J. D. (2000) Enstatite–forsterite–water equilibria at elevated temperatures and pressures. *Am. Mineral.* **85**(7–8), 918–925.

Associate editor: Bjorn Mysen